

Adsorption of methyl orange and methylene blue on activated biocarbon derived from birchwood pellets

Original

Adsorption of methyl orange and methylene blue on activated biocarbon derived from birchwood pellets / Lee, Heejin; Fiore, Silvia; Berruti, Franco. - In: BIOMASS & BIOENERGY. - ISSN 0961-9534. - ELETTRONICO. - 191:(2024). [10.1016/j.biombioe.2024.107446]

Availability:

This version is available at: 11583/2993690 since: 2024-10-25T11:35:04Z

Publisher:

Elsevier

Published

DOI:10.1016/j.biombioe.2024.107446

Terms of use:

This article is made available under terms and conditions as specified in the corresponding bibliographic description in the repository

Publisher copyright

Elsevier postprint/Author's Accepted Manuscript

© 2024. This manuscript version is made available under the CC-BY-NC-ND 4.0 license
<http://creativecommons.org/licenses/by-nc-nd/4.0/>. The final authenticated version is available online at:
<http://dx.doi.org/10.1016/j.biombioe.2024.107446>

(Article begins on next page)



Adsorption of methyl orange and methylene blue on activated biocarbon derived from birchwood pellets

Heejin Lee ^a, Silvia Fiore ^{a,b}, Franco Berruti ^{a,*}

^a Institute for Chemicals and Fuels from Alternative Resources, Faculty of Engineering, Western University, London, Ontario, Canada

^b DIATI (Department of Engineering for Environment, Land, and Infrastructure), Politecnico di Torino, Corso Duca Degli Abruzzi 24, Torino, 10129, Italy

ARTICLE INFO

Keywords:

Adsorption
Biochar
Biocarbon
Isotherm
Kinetics
Dye
Methylene blue
Methyl orange

ABSTRACT

This study explored the adsorption capacity of a physically activated biocarbon derived from the pyrolysis of birchwood pellets (ABPB) towards two dyes - methyl orange (MO, anionic) and methylene blue (MB, cationic), at pH 2, 7 and 11. Compared to mineral commercial activated carbon (CAC_{mineral}), ABPB exhibited lower SSA, pores volume and surface; higher external surface and average pore diameter, similar ash content and aromaticity, and stronger hydrophilicity and polarity. The maximum adsorption capacity on ABPB was equal to 220 mg/g for MO and 91 mg/g for MB after 17 h. Batch tests with variable adsorbent amount (0.5–2.5 g/L) showed for both ABPB and CAC_{mineral} better results for lower adsorbent dose. Under all tested conditions, ABPB showed higher or analogous adsorption capacity compared to CAC_{mineral}. Based on the pK_a of MB (3.80) and MO (3.46) and on the pH_{PZC} of ABPB (5.3), the adsorption was favored at pH 2 for MO and at pH 11 for MB. Kinetics analysis and isotherm modelling revealed that, although many different physicochemical interactions occurred between ABPB and the dyes molecules, chemisorption is the rate-controlling step and prevalent mechanism. In conclusion, this study may provide support to further research aimed at exploring the effect of ABPB's physicochemical properties on the efficiency and mechanisms of dyes adsorption.

1. Introduction

Dyes occur in wastewater derived from various industrial sectors, including paper, textile, leather, and printing [1]. Among wastewater treatments applicable for dyes removal, adsorption on commercial activated carbon (CAC) stands out due to its superior efficacy compared to membrane filtration, photocatalysis, oxidation, and coagulation [2]. CACs, porous carbon materials with a non-graphitic structure [3], are widely used as adsorbents because of their large specific surface area (SSA), pore distribution, and micro-mesoporous structures. CAC's high cost is a significant barrier to its wider application [4]. CAC production has relevant environmental impacts due to its energy-intensive manufacturing and the use of precursors often concentrated in Southeast Asia, leading to long transport routes [5].

Biocarbon (BC), often also called 'biochar' when utilized in agronomy as soil amendment, is the carbonized solid co-product derived from the pyrolysis of waste biomass and it has been shown to offer a promising alternative to CAC as sustainable adsorbent [6]. BC has gained popularity in wastewater treatment because of its peculiar

physicochemical characteristic (large SSA, porosity, diverse functional groups, and mineral components) [7], which are influenced by the source biomass and pyrolysis operating conditions [8]. To achieve adsorption capacities comparable to CAC, BC can be activated through physical or chemical methods [9], improving SSA and pore structure. In this paper, the activated form of biocarbon is referred to as ABC. Chemical activation often involves strong alkali or acidic agents [10], while physical activation uses CO₂ or steam at temperatures up to 900 °C [11]. This is considered more environmentally friendly and cost-effective compared to chemical activation, as it avoids the use of harsh chemicals and relies on physical processes [12].

ABC's ability to adsorb dyes has been previously explored (Table 1), focusing on methylene blue (MB), a cationic dye [13], and methyl orange (MO), an anionic azo dye [14], as target compounds. Various types of biomasses, including wood residues, leaves, and fruit peels, have been used as starting materials, with pyrolysis carried out at temperatures between 280 °C and 800 °C. The activation of biocarbon was conducted either chemically, using inorganic or organic agents, or physically, using CO₂. The SSA of the produced ABC ranged from 100 to 900 m²/g (with

* Corresponding author. Institute for Chemicals and Fuels from Alternative Resources, Faculty of Engineering, Western University, Ontario, Canada, 22312, Wonderland Rd N., Ilderton, ON N0M 2A0, Canada.

E-mail address: fberruti@uwo.ca (F. Berruti).

<https://doi.org/10.1016/j.biombioe.2024.107446>

Received 6 September 2024; Received in revised form 15 October 2024; Accepted 17 October 2024

0961-9534/© 2024 The Authors. Published by Elsevier Ltd. This is an open access article under the CC BY license (<http://creativecommons.org/licenses/by/4.0/>).

Table 1

Overview of literature data regarding the adsorption of methylene blue (MB) and methyl orange (MO) onto activated biocarbon (ABC), with details about ABC's features (Biomass, pyrolysis temperature, activation agent, specific surface area SSA, and adsorption capacity) (N.A.*: not available).

Dye	Biomass	Pyrolysis temperature (°C)/time (min)	Activation agent	SSA (m ² /g)	Adsorption capacity (mg/g)	Reference
MB	Ginkgo leaves	500/120	Steam	503.05	111.63	[1]
	Beech wood residue	650/15	Citric acid	146	117.33	[14]
	Eucalyptus camdulensis	800/180	Not applied	N.A.*	123.33	[17]
	Areca residue	600/150	NaOH	105	152.72	[18]
	Pine sawdust	800/60	CO ₂	906.44	197.47	[19]
	Medulla tetrapanacis	600/60	KCl	307.28	228.62	[20]
	Water hyacinth	300/120	Citric acid	57.08	395	[21]
	Wood sawdust	280/240	H ₂ SO ₄	2.88	643.74	[22]
MO	Neem chips	800/120	FeCl ₃	N.A.*	80.30	[23]
	Pomelo peel waste	450/60	H ₃ PO ₄	75.32	147.87	[24]
	Date palm frond waste	700/240	Not applied	431.82	163.13	[25]
	<i>Moringa oleifera</i> leaves	350/120	H ₃ PO ₄	267.15	175.05	[26]
	Egyptian doum palm shells	500/120	NaOH	33.38	264.92	[27]

few references reporting values below 100 m²/g), leading to adsorption capacity of 117–643 mg/g for MB and of 80–175 mg/g for MO. About the comparison of ABC and CAC performances towards the adsorption of MB, Dang et al. (2023) [15] investigated KOH-activated rice husk activated carbon (KN-AC) and CAC for MB. Within the pH range from 2 to 10, KN-AC exhibited adsorption capacity increasing from 303.5 mg/g to 359.5 mg/g as pH increased from 2 to 8. CAC exhibited a similar trend, with adsorption capacity topping 173.3 mg/g at pH 8. Serban et al. (2023) [16] reported the maximum adsorption capacity of CAC for MO equal to 129.3 mg/g.

Several studies have explored the influence of pH on dye adsorption, demonstrating that pH can affect both the surface charge of the adsorbent and the ionization state of the dye molecules. For instance, at lower pH values, the surface of ABC tends to become more positively charged, enhancing the adsorption of anionic dyes like MO through electrostatic attraction. Conversely, at higher pH values, the surface becomes more negatively charged, which is more favorable for adsorbing cationic dyes like MB. Zeghioud et al. (2022) [14] reported that cationic dyes achieve optimal adsorption at pH values above 6, particularly when the pH is higher than the p*H*_{pzc} of the adsorbent. They attributed the lower adsorption capacity at low pH to the predominance of undissociated MB molecules, since the p*K*_a of MB is lower than the pH, and the adsorbent surface remains positively charged. Similarly, Zhang et al. (2020) [24] found that the highest adsorption capacity for MO occurred at pH 3, attributing this to the strong electrostatic attraction between the negatively charged SO₃⁻ groups of MO molecules and the positively charged adsorbent surface under acidic conditions.

However, there is limited literature that clearly identifies which ABC characteristics more significantly influence dye adsorption performance. This gap in knowledge is particularly relevant for applications involving varying pH levels, which can impact both the physical and chemical properties of the adsorbent and adsorbate. To address this gap, this study explores the adsorption capacity of ABC towards dyes at different pH values with a focus on its physicochemical properties. In detail, ABC was produced from the slow pyrolysis at 500 °C of a lignocellulosic biomass (birchwood pellets) and physically activated with CO₂ at 900 °C. This product was named ABPB. The ABPB's features were investigated: SSA, pore size and volume, ash and moisture contents, %-wt of C, H, N and S, identity of surface functional groups, and point of zero charge. To

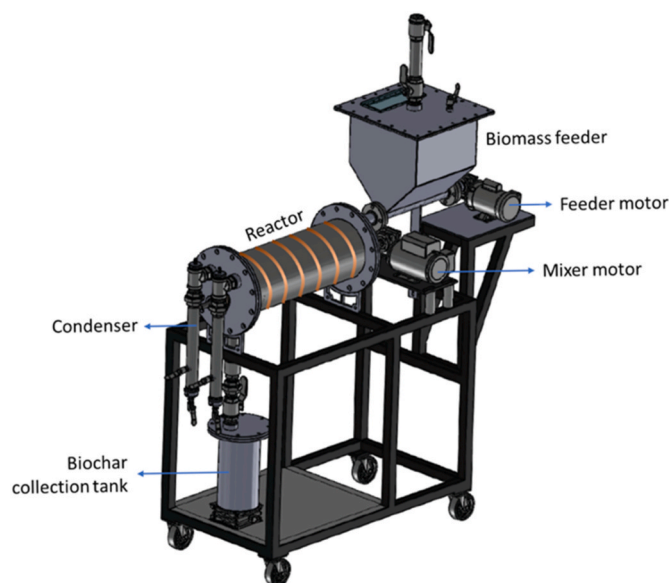
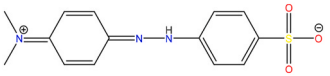
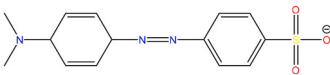
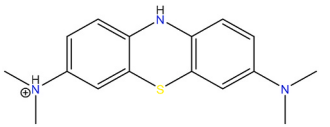
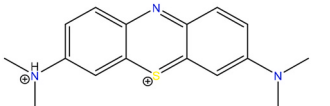


Fig. 1. Outline of the pyrolysis rotating horizontal reactor (PYROH).

provide results directly comparable with existing literature, MO and MB were chosen as reference dyes. The results of batch tests applying different dosages of ABPB and pH values were analyzed to investigate the adsorption performance utilizing different kinetic and isotherm models. This study includes a novel comparative analysis of ABPB and CAC_{mineral} adsorption capabilities, highlighting key insights into ABPB's potential as an eco-friendly, cost-effective adsorbent for wastewater treatment. The novelty of this study lies in its comprehensive analysis of ABPB's adsorption performance towards dyes at different pH levels, while systematically comparing it to CAC_{mineral}, and investigating how specific physicochemical properties of ABPB influence its efficiency as a sustainable adsorbent.

Table 2
Some properties of methylene blue (MB) and methyl orange (MO) [14,24,29].

Dye	Molecular formula	Molar mass (g/mol)		Molecular structure	Solubility at 25 °C (mg/L)	pK _a
MO	C ₁₄ H ₁₄ N ₃ NaO ₃ S	327.33	pH < pK _a		5000	3.46
			pH > pK _a			
MB	C ₁₆ H ₁₈ ClN ₃ S	319.85	pH < pK _a		43,600	3.80
			pH > pK _a			

2. Materials and methods

2.1. Materials and characterization

Commercial Activated Carbon derived from minerals (CAC_{mineral}) was purchased from Amtra (Castronno, Italy). Birchwood pellets bio-carbon (BPB) was produced via a pyrolysis rotating horizontal pilot plant reactor (PYROH) (Fig. 1), operated at pressure below 5 psi and temperature between 450 and 500 °C, and fed with 0.3 kg/min of birchwood pellets purchased from Northern Flame (St. Catharines, Ontario, Canada). Physical activation was performed in a 1.3 m long horizontal fixed bed tube furnace equipped with three heating zones (Across International, New Jersey, USA). A heating rate of 10 °C/min was used to reach 900 °C, maintained for 3 h, and injecting a constant flow of CO₂ gas at 2 L/min. The residence time of the CO₂ activation gas in the tube furnace was approximately 1.3 min. The activated BPB was labeled as ABPB.

The physicochemical characterization of ABPB included the following parameters (all tests conducted in triplicate): SSA and porosity, measured via Brunauer-Emmett-Teller (BET) analysis with liquid nitrogen at -196 °C using a Nova 2000e surface area and pore size analyzer (Quantachrome Instrument, Anton Paar Quanta Tec Inc., Florida, USA); content of ash through proximate analysis (ASTM D1762-84 standard); surface functional groups (and therefore aromaticity, hydrophilicity, and polarity of ABPB) were identified via the H/C, O/C, and (O + N)/C atomic ratios [28] using a Fourier-Transform Infrared (FTIR) spectrometer (PerkinElmer, Massachusetts, USA); zeta potential via a Zetasizer Nano ZSP, Malvern Panalytical, Worcestershire, UK; the elemental analysis of the adsorbents using an EA 1112 Series CHNS elemental analyzer (Thermo Fisher Scientific, Massachusetts, USA). The elemental composition of the adsorbent samples was determined using Inductively Coupled Plasma Optical Emission Spectroscopy (ICP-OES). The samples were sent to PPB Analytical, Inc. (Toronto, Ontario, Canada), where the analysis was performed. The resulting data provided concentrations of key elements, including aluminum, barium, calcium, chromium, copper, iron, manganese, molybdenum, nickel, phosphorous, sulfur, and tin.

All chemical reagents were of analytical grade. Methyl Orange (MO) was purchased from Sigma-Aldrich (Burlington, Massachusetts, USA). Methylene Blue (MB) was purchased from Caledon Laboratories Ltd. (Georgetown, Ontario, Canada). Some characteristics of MO and MB are shown in Table 2.

2.2. Adsorption tests

The batch tests involved 50 mL of MO and MB 500 ppm stock solution, with ABPB or CAC_{mineral} doses ranging from 0.5 to 2.5 g/L and pH equal to 2, 7, and 11. The tests were performed in triplicates at 293 K. The samples were filtered through 0.22 μm membranes (Maple Lab Systems, Mississauga, Canada) before measuring the residual dyes concentration using a UV spectrophotometer (Evolution 220, Thermo-Scientific, Massachusetts, USA) at 464 nm for MO and 668 nm for MB [25,30]. The equilibrium contact time was experimentally measured via tests involving MO and MB and 1 g/L of ABPB. The adsorption capacity of each adsorbent q_e (mg/g) and the removal percentage were calculated according to eqs. (1) and (2):

$$\text{Adsorption capacity (mg / g)} = q_e = \frac{(C_0 - C_e) \times V}{M} \quad (1)$$

$$\text{Percentage removal (\%)} = \frac{(C_0 - C_e)}{C_0} \times 100 \quad (2)$$

where q_e : equilibrium uptake capacity of adsorbent (mg/g), C_0 : initial concentration (mg/L) of adsorbate, C_e : equilibrium concentration (mg/L) of adsorbate, V : volume of adsorbate solution (L), and M : adsorbent dosage (g).

2.3. Adsorption kinetic modeling

The pseudo-first order (PFO) kinetic, pseudo-second order (PSO) kinetic, Elovich, and intraparticle diffusion (ID) models were applied. The PFO kinetic model assumes that adsorption rate is proportional to the quantity of unoccupied sites [24], and predominantly controlled by physisorption [31]. The PSO kinetic model assumes that adsorption is a chemical reaction involving creation of covalent bonds between adsorbent and adsorbate [32,33]. The Elovich kinetic model refers to multi-layer chemisorption [34,35]. However, while the aforementioned models are frequently used to depict the overall trend of the adsorption process, they are ineffective in describing the variations in the adsorption rate within the process [24]. For this reason, the ID model has been implemented to conduct a more comprehensive analysis of the adsorption kinetics by identifying different phases of mass transfer. The ID model describes diffusion process of adsorbates inside the adsorbent pores, and it can also be used to identify the rate-controlling step of the adsorption process [24].

Table 3

Results of BET analysis of birchwood pellet biocarbon (BPB), activated birchwood pellet biocarbon (ABPB) and mineral commercial activated carbon (CAC_{mineral}) (S: surface, V: volume).

Adsorbent	SSA ($\text{m}^2 \cdot \text{g}^{-1}$)	S_{micro} ($\text{m}^2 \cdot \text{g}^{-1}$)	S_{ext} ($\text{m}^2 \cdot \text{g}^{-1}$)	V_{total} ($\text{cm}^3 \cdot \text{g}^{-1}$)	V_{micro} ($\text{cm}^3 \cdot \text{g}^{-1}$)	Average pore diameter (nm)
BPB	5.34	–	–	–	–	–
ABPB	437.34	362.46	74.88	0.2702	0.188	1.24
CAC_{mineral}	584.97	513.95	71.03	0.3317	0.258	1.13

Table 4

Elemental composition and ash content of activated birchwood pellet biocarbon (ABPB) and mineral commercial activated carbon (CAC_{mineral}) (DL: Detection Limit).

Adsorbents	Ash [%]	Elemental analysis					Atomic ratio			
ABPB	14.25	76.62	0.05	<DL	<DL	9.09	0.001	0.119	0.119	
CAC_{mineral}	13.51	79.16	<DL	3.91	<DL	3.41	<DL	0.043	0.093	

Table 5

Elemental composition of activated birchwood pellet biocarbon (ABPB) and mineral commercial activated carbon (CAC_{mineral}) determined by ICP-OES.

Analyte (ppm)	ABPB	CAC_{mineral}
Aluminum (Al)	618.9	1006.2
Antimony (Sb)	N.D. ^a	N.D.
Arsenic (As)	N.D.	N.D.
Barium (Ba)	309.8	72.3
Beryllium (Be)	N.D.	<LOQ ^b (0.007)
Cadmium (Cd)	N.D.	N.D.
Calcium (Ca)	25004.3	4828.2
Chromium (Cr)	232.6	<LDQ (0.014)
Copper (Cu)	37.3	N.D.
Iron (Fe)	40916.1	451.8
Lead (Pb)	N.D.	N.D.
Manganese (Mn)	3981.0	19.6
Molybdenum (Mo)	452.7	14.7
Nickel (Ni)	11904.2	54.6
Phosphorous (P)	5839.2	667.3
Selenium (Se)	N.D.	N.D.
Sulfur (S)	412.9	170.1
Tin (Sn)	103.7	N.D.
Vanadium (V)	<LOQ (0.101)	<LOQ (0.101)
Zinc (Zn)	N.D.	N.D.

^a N.D.: Not detected.

^b LDQ: Limit of quantification.

2.4. Adsorption isotherm modeling

Langmuir, Freundlich, and Temkin models were applied [36]. Langmuir model postulates a monolayer adsorption mechanism and homogeneous adsorbent surface [37]. Freundlich model describes a multilayer adsorption process and adsorbent surface heterogeneity [38]. Temkin model postulates that the reduction in adsorption energy on the adsorbent surface is a result of the interaction between the adsorbate and the adsorbent [24], and it also suggests that this reduction is directly proportional to the surface coverage rate.

3. Results and discussion

3.1. Characterization of the adsorbents

Activation increased SSA of BPB from 5.3 m^2/g to 437.3 m^2/g (Table 3). ABPB, compared to CAC_{mineral} , showed in overall lower SSA, micropores surface (S_{micro}), total pore volume (V_{total}) and micropores volume (V_{micro}), and higher external surface (S_{ext}) and average pore diameter. Based on IUPAC categorization [39], the nitrogen adsorption-desorption isotherms of ABPB and CAC_{mineral} correspond to type I isotherms, observed in microporous (<2 nm) materials with limited S_{ext} [40].

The elemental components in ABPB and CAC_{mineral} were also analyzed by ICP-OES, as shown in Table 5. This analysis reveals significant differences in the concentrations of various minerals between ABPB and CAC_{mineral} , indicating varying adsorption capacities and mineral compositions. Calcium, iron, manganese, nickel, and

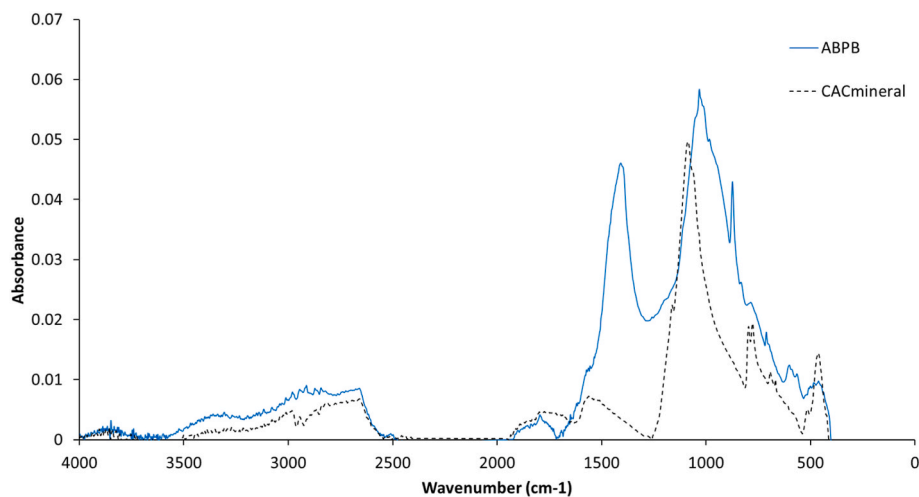


Fig. 2. Identification of surface functional groups on activated birchwood pellet biocarbon (ABPB) and mineral commercial activated carbon (CAC_{mineral}) via FTIR analysis.

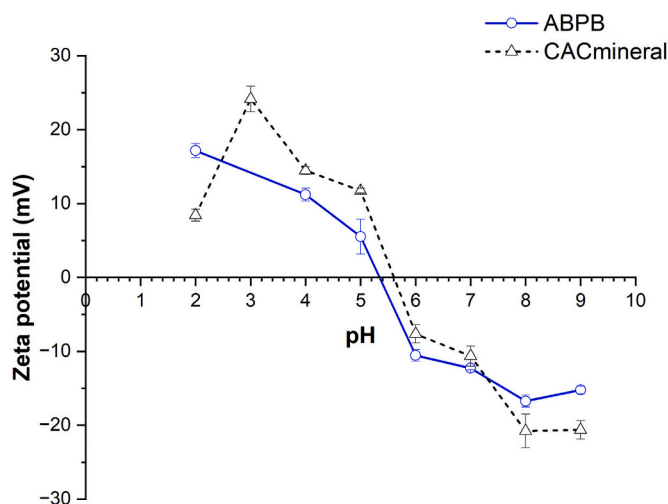


Fig. 3. Zeta potential trends of activated birchwood pellet biocarbon (ABPB) and mineral commercial activated carbon (CAC_{mineral}).

phosphorous were the main mineral components found in the ABPB, while aluminum and calcium were the main mineral components found in CAC_{mineral}. The aluminum (Al) content was notably higher in CAC_{mineral} compared to ABPB, which may contribute to its structural properties [41]. The calcium and manganese contents were also much higher in ABPB compared to CAC_{mineral}. Calcium and magnesium are important components in the biocarbon, enhancing its chemical adsorption processes. These elements, particularly in their oxide forms, contribute to the basicity of the biocarbon's surface, enhancing its ability to attract acidic pollutants like MO. The presence of these minerals in the biocarbon leads to mechanisms such as electrostatic interactions, cation exchange, and surface complexation promoting the adsorption of negatively charged pollutants [41,42]. Singh et al. (2022) [43] observed that the release of cations like Ca²⁺ from biocarbon in aqueous solutions suggests ion exchange as a mechanism for dye adsorption. The calcium content is much higher in ABPB than in CAC_{mineral}. This explains higher adsorption capacity of MO onto ABPB despite of lower surface area and porosity.

ABPB and CAC_{mineral} showed similar ash content (Table 4), while ABPB displayed lower SSA and S_{micro} compared to CAC_{mineral} (Table 3). The ash content might be attributed to inorganic mineralization during pyrolysis and contaminants in the parent biomass [44]. A significant ash content (>20 %) may hinder the formation of micro and mesopores [45] and SSA increase during activation. Sewu et al. (2017) [46] demonstrated that high ash content in ABC increased its ion exchange capacity, as inorganic minerals in the ash provide additional active sites for adsorption. This is effective for cationic compounds, such as MB, due to the attraction between the positively charged dye molecules and the negatively charged functional groups on ABC surface.

The aromaticity, hydrophilicity, and polarity of adsorbents can be assessed by analyzing the H/C, O/C, and (O + N)/C atomic ratios, respectively [28]. As H/C ratio decreases, the carbonation level and aromaticity increase. An increase in O/C atomic ratio corresponds to higher hydrophilicity, while a rise in (O + N)/C atomic ratio results in increased polarity. Both ABPB and CAC_{mineral} have high levels of aromaticity and carbonization due to very low H/C ratios (Table 4). Despite their similar aromaticity, higher O/C and (O + N)/C ratios of ABPB indicate stronger hydrophilicity and polarity compared to CAC_{mineral}. This is confirmed by the analysis of the surface functional groups on ABPB and CAC_{mineral} (Fig. 2). The broad band around 2600–3000 cm⁻¹ is attributed to O-H stretching of the carboxylic acid functional group [47]. The peaks at 1700–1900 cm⁻¹ are associated with stretching vibrations of the carbonyl group (C=O) [7]. Peaks between 1300 cm⁻¹ and 1600 cm⁻¹ indicate a C=C-C stretch, a feature of an aromatic ring

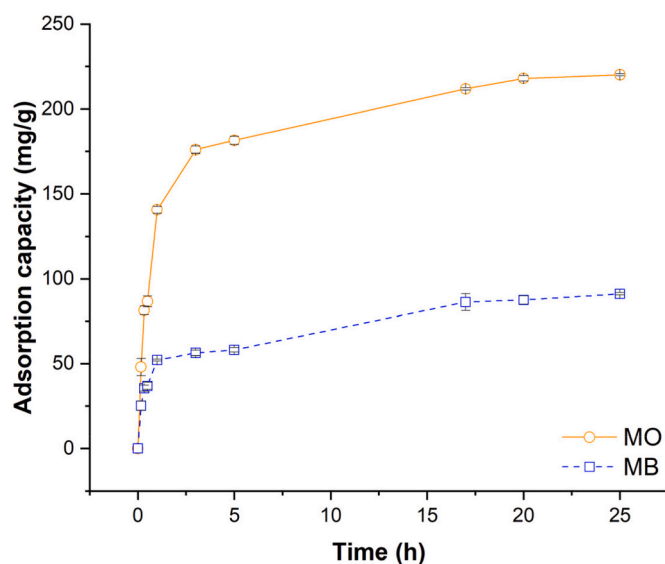


Fig. 4. Effect of time on methyl orange (MO) and methylene blue (MB) adsorption on activated birchwood pellet biocarbon (ABPB). (For interpretation of the references to colour in this figure legend, the reader is referred to the Web version of this article.)

structure [48]. The peaks at 1030 cm⁻¹ show the presence of C-O stretching [14]. The presence of a peak at 440 cm⁻¹ corresponds to aromatic C-H stretching [49].

The point of zero charge (pH_{pzc}) is a key parameter for the analysis of any adsorbent surface charge properties [24] and therefore to possible electrostatic attraction. The adsorbent surface is protonated and positively charged when pH value is lower than pH_{pzc}; otherwise, it is deprotonated and negatively charged [50]. Positively charged adsorbent surface promotes the uptake capacity of anion pollutants (as MO), while negatively charged adsorbent surface favors the adsorption of cationic species (as MB). According to the electric charge properties of the adsorbent surfaces and of the dyes at different pH values, the solution can be modulated to the optimal pH value to increase the adsorption performance of the adsorbents for each dye removal. The pH_{pzc} values of ABPB and CAC_{mineral} were 5.3 and 5.6, respectively (Fig. 3).

3.2. Adsorption tests

Considering the effect of contact time on MO and MB adsorption onto ABPB (Fig. 4), the adsorption capacity rapidly increased and then stabilized over 17 h, reaching an equilibrium at 220.2 mg/g for MO and 91.1 mg/g for MB. This is due to the high dye concentration and the abundance of available adsorption sites on ABPB surface during the initial adsorption stage [48]. The dyes quickly occupy the available adsorption sites because of the concentration gradient between the liquid and solid interfaces, resulting in a substantial increase in adsorption capacity. As adsorption progresses, the quantity of available adsorption sites diminishes, and the driving force generated by the concentration gradient becomes progressively weaker. This makes it more difficult for additional dyes to overcome the mass transfer resistance and adhere to the adsorbent surface. Subsequently, the adsorption capacity stabilized, and the adsorption rate slowed progressively until equilibrium was reached.

The influence of the adsorbent dosage was examined (Fig. 5), observing for both ABPB and CAC_{mineral} that an increase in the adsorbent quantity led to a reduction in the amount of dye adsorbed per unit mass of adsorbent. This was due to an excessive dose of adsorbent, which led to a reduction in the quantity of dye adsorbed per unit mass of adsorbent [44]. In contrast, the removal rate rose as the dosage of the adsorbent increased, as higher dosage of adsorbent leads to an increase in the

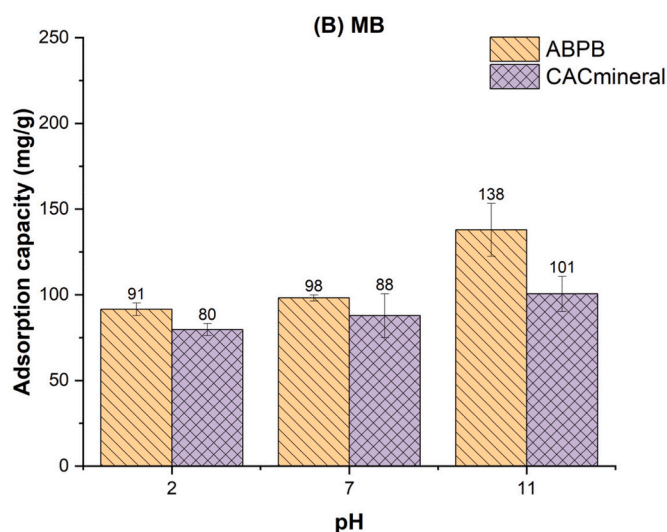
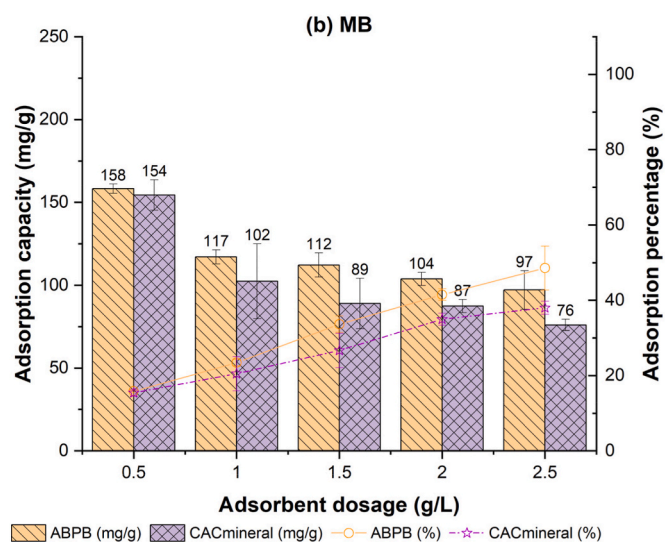
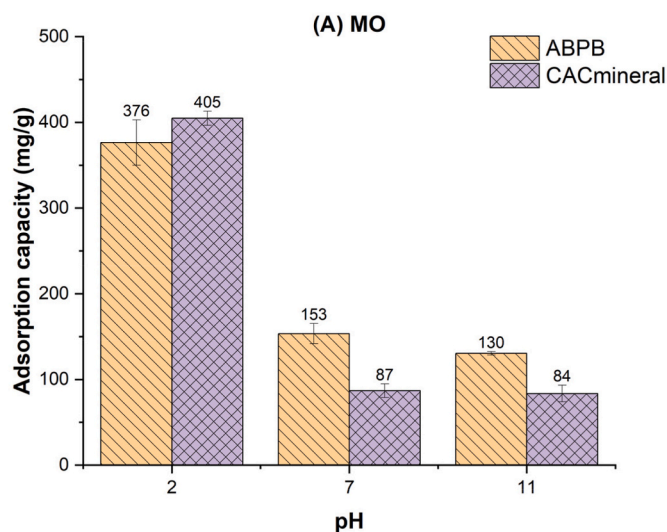
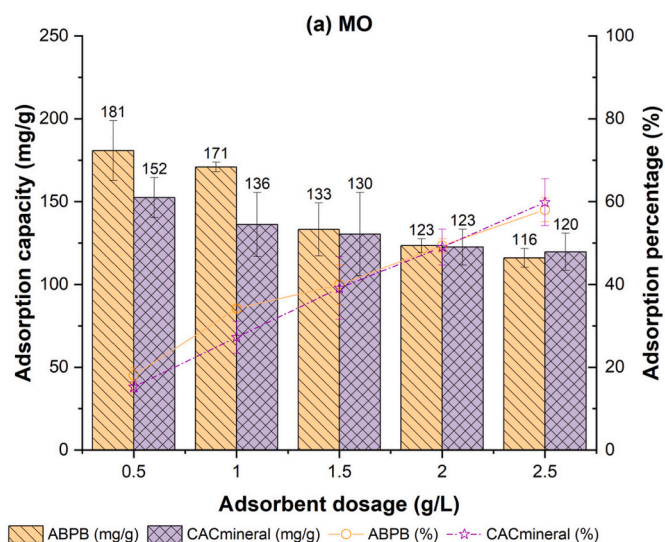


Fig. 5. Effect of adsorbent dosage on (a) methyl orange (MO) and (b) methylene blue (MB) adsorption capacity of activated birchwood pellet biocarbon (ABPB) and mineral commercial activated carbon (CAC_{mineral}). (For interpretation of the references to colour in this figure legend, the reader is referred to the Web version of this article.)

number of adsorption sites available to bond with more adsorbates, hence improving the removal rate of dyes [24]. Varying sorbent dose, compared to CAC_{mineral}, ABPB showed higher or analogous adsorption capacity for MO and higher capacity for MB.

Fig. 6 displays the trends of adsorption capacity at different pH values using an adsorbent dose of 1 g/L, which led to define pH 2 and 11, respectively, as optimal values for MO and MB adsorption on ABPB and CAC_{mineral}. In details, MO adsorption peaked at pH 2 with 376 mg/g on ABPB and 405 mg/g on CAC_{mineral}, then declined to 130 mg/g on ABPB and 83 mg/g on CAC_{mineral} at pH 11 (Fig. 6A). This suggests that the adsorption of an anionic dye (as MO) onto ABPB is favored under acidic conditions [25], when MO includes Na⁺ ions and positive groups carried by -SO³⁻, and it exhibits zwitterionic properties when pH is lower than its pK_a value (3.46) [51]. When pH is below the pH_{pzc} of the adsorbents, their functional groups will undergo protonation by reacting with H⁺ ions. As a result, a strong electrostatic interaction between the negatively charged MO and the positively charged adsorbent surface facilitated adsorption at low pH values. On the other hand, the protonation on

Fig. 6. Effect of pH on (a) methyl orange (MO) and (b) methylene blue (MB) adsorption capacity of activated birchwood pellet biocarbon (ABPB) and mineral commercial activated carbon (CAC_{mineral}). (For interpretation of the references to colour in this figure legend, the reader is referred to the Web version of this article.)

the adsorbent surface decreased when pH increased, leading to the development of a negative charge on the adsorbent surface, as indicated by the zeta potential. Also, MO loses Na⁺ ions and carries only -SO³⁻ ions above its pK_a value. Thus, the negatively charged adsorbent and MO experienced electrostatic repulsion, leading to a decrease in the adsorption capacity. Moreover, OH⁻ concentration increased with pH, resulting in a competition for adsorption between OH⁻ ions and the negatively charged dye. Consequently, in overall, for MO the adsorption capacity decreased when pH increased.

Considering MB, adsorption increased with pH (Fig. 6B): at pH 11, the adsorption capacities of ABPB and CAC_{mineral} were 138 mg/g and 101 mg/g, respectively, compared to 91 and 80 mg/g at pH 2. This happened because of the cationic nature of MB [28]. Under acidic conditions the adsorbent surface can become highly protonated and positively charged, causing electrostatic repulsion with cationic MB. On the contrary, increasing pH leads to a decrease in H⁺ ions competing for adsorption, resulting in enhanced adsorption capacity. At high pH, the

Table 6

Adsorption kinetic parameters for methylene blue (MB) and methyl orange (MO) on activated birchwood pellet biocarbon (ABPB) (q_e : adsorption capacity ($\text{mg}\cdot\text{g}^{-1}$) at equilibrium, k_1 (min^{-1}) is the pseudo-first order rate constant, k_2 ($\text{g}\cdot\text{mg}^{-1}\cdot\text{min}^{-1}$) is the pseudo-second order rate constant, α ($\text{mg}\cdot\text{g}^{-1}\cdot\text{min}^{-1}$) is the initial adsorption rate, β ($\text{g}\cdot\text{mg}^{-1}$) denotes desorption constant, which is inversely related to the extent of surface coverage and the activation energy for chemisorption, C ($\text{mg}\cdot\text{g}^{-1}$) is the intercept, which is related to boundary layer thickness, k_{id} ($\text{mg}\cdot\text{g}^{-1}\cdot\text{min}^{-1/2}$) is the intraparticle diffusion rate constant).

Kinetic model			MB	MO
	q_e (exp) ($\text{mg}\cdot\text{g}^{-1}$)		91.13	220.19
Pseudo-first order	q_e (cal) ($\text{mg}\cdot\text{g}^{-1}$)		76.13	203.90
	k_1 (min^{-1})		0.02	0.02
	R^2		0.7466	0.9467
Pseudo-second order	q_e (cal) ($\text{mg}\cdot\text{g}^{-1}$)		83.52	220.77
	$k_2 \times 10^{-3}$ ($\text{g}\cdot\text{mg}^{-1}\cdot\text{min}^{-1}$)		0.31	0.11
	R^2		0.8532	0.9811
Elovich	α ($\text{mg}\cdot\text{g}^{-1}\cdot\text{min}$)		7.83	16.53
	B ($\text{mg}\cdot\text{g}^{-1}$)		0.08	0.03
	R^2		0.9465	0.9651
Intraparticle diffusion	C_1 ($\text{mg}\cdot\text{g}^{-1}$)		6.53	5.15
	$k_{id,1}$ ($\text{mg}\cdot\text{g}^{-1}\cdot\text{min}^{-1/2}$)		5.77	14.69
	R^2		0.8020	0.9310
	C_2 ($\text{mg}\cdot\text{g}^{-1}$)		34.52	109.41
	$k_{id,2}$ ($\text{mg}\cdot\text{g}^{-1}\cdot\text{min}^{-1/2}$)		1.52	4.41
	R^2		0.9499	0.9031
	C_3 ($\text{mg}\cdot\text{g}^{-1}$)			176.07
	$k_{id,3}$ ($\text{mg}\cdot\text{g}^{-1}\cdot\text{min}^{-1/2}$)			1.16
	R^2			0.7790

adsorbent surface undergoes deprotonation, facilitating the electrostatic attraction towards MB cations. Consequently, overall, for MB the adsorption capacity increased when pH increased.

3.3. Kinetics modelling

The results of the kinetics modelling are in Table 6 and in Figs. 7–8. For MO, the PSO model exhibited a stronger correlation coefficient ($R^2 > 0.981$) compared to PFO ($R^2 > 0.947$) and Elovich ($R^2 > 0.965$). PSO model predicted the q_e value of ABPB for MO (220.8 mg/g), consistently with the experimental equilibrium capacity (220.2 mg/g) (section 3.2). These kinetic findings suggest that MO adsorption onto ABPB involves chemisorption– π - π interactions, electrostatic interactions, and chemical reactions between ABC surface and MO molecules [25]. For MB, the Elovich model exhibited a greater correlation coefficient ($R^2 > 0.947$) compared to PFO ($R^2 > 0.747$) and PSO ($R > 0.853$). This suggests that chemisorption played a major role in MB adsorption on ABPB, as Elovich model describes adsorption as a heterogeneous diffusion process controlled by reaction rate and diffusion exert [52].

Applying the ID model (Fig. 8), three distinct phases of adsorption on ABPB were identified for MO and two phases for MB (Table 6). For both dyes, the value of $k_{id,1}$ i.e., the steeper slope of the initial stage in Fig. 8, is greater than those of $k_{id,2}$ and $k_{id,3}$. The adsorption process can be described as follows. During the initial phase (i.e., film diffusion), the adsorption sites on ABPB rapidly become saturated with the adsorbate. During this phase, the rapid rate of adsorption is influenced by chemical interactions, including electrostatic and chemical bonding, facilitated by the abundant supply of active bonding sites (oxygen functionalities) on ABC surface. During the second phase (i.e., intraparticle diffusion), the dye molecules interact with the adsorption sites located within the pores of the adsorbent, and pore diffusion happens. The increased mass transfer resistance of these hinders the diffusion of dyes, and the rate constant is minor than previous stage. The final phase (i.e., active site saturation) occurs when equilibrium is reached. In addition, the fitting lines fail to pass through the origin point in Fig. 8, indicating that diverse adsorption mechanisms are involved.

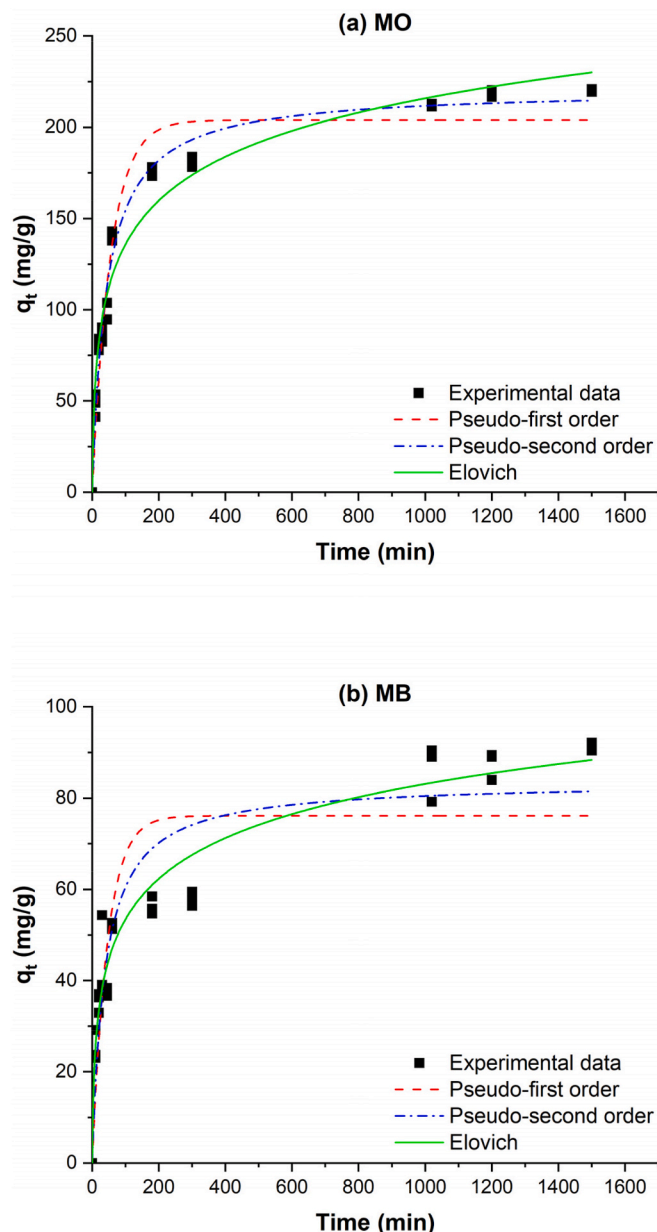


Fig. 7. Non-linear adsorption kinetics fitting plots for (a) methyl orange (MO) and (b) methylene blue (MB) on activated birchwood pellet biocarbon (ABPB). (For interpretation of the references to colour in this figure legend, the reader is referred to the Web version of this article.)

3.4. Isotherms modelling

The experimental data were fitted via Langmuir, Freundlich, and Temkin adsorption isotherm models (Table 7). Freundlich model displayed higher coefficient, suggesting that adsorption onto ABPB happened through multiple layers on a heterogeneous adsorbent surface. K_F indicates the affinity between the adsorbent and adsorbate, and the values calculated for MO and MB adsorbed by ABPB were 38.46 and 40.25, respectively. $1/n$ is commonly employed in the assessment of adsorption control [37], and the values calculated for MO (0.2580) and MB (0.1480) fall within the range of 0.1–1 [53], typical of favorable adsorption.

3.5. Discussion of the adsorption mechanisms

Based on the obtained results, MO and MB adsorption onto ABPB

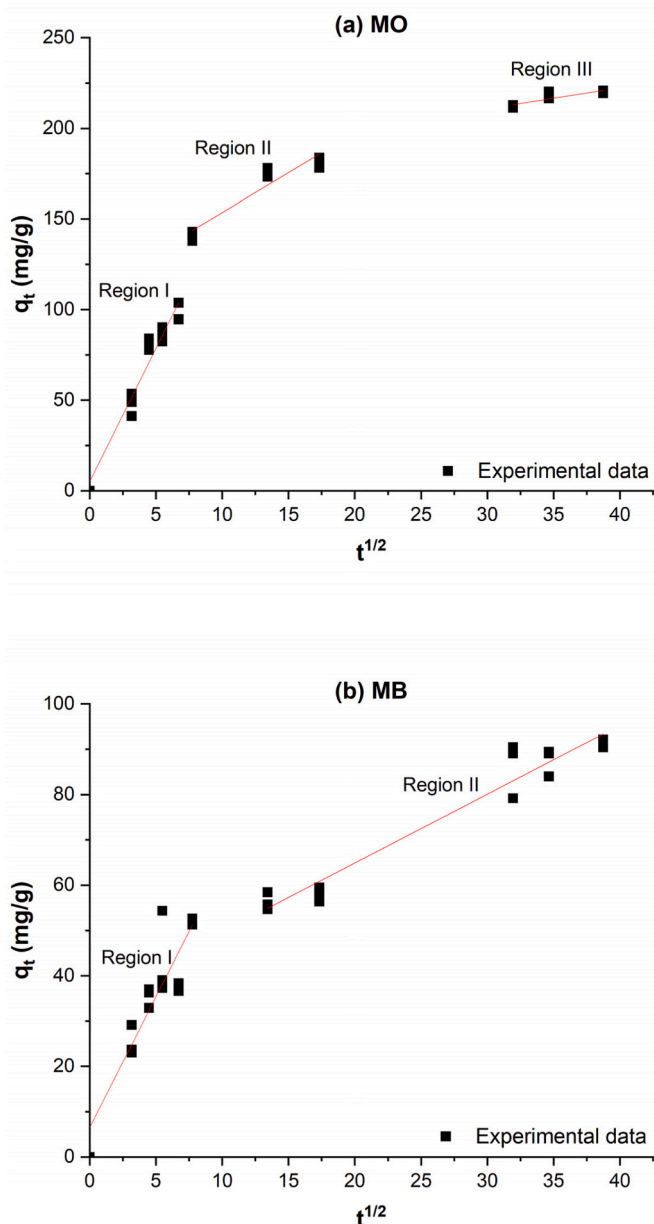


Fig. 8. Intraparticle diffusion kinetic model of (a) methyl orange (MO) and (b) methylene blue (MB) on activated birchwood pellet biocarbon (ABPB). (For interpretation of the references to colour in this figure legend, the reader is referred to the Web version of this article.)

happened involving physical and chemical adsorption, with chemical adsorption as predominant mechanism. MO adsorption followed the PSO kinetic model, indicating that chemisorption is the rate-controlling step. Physical adsorption also happened, involving electrostatic interactions between the positively charged surface (i.e., H^+) of ABPB and the negatively charged group (i.e., SO_3^-) on MO [40], with adsorption capacity of ABPB enhanced at low pH values. Increasing pH, the protonation on ABPB surface gradually decreases, and a negative charge develops for pH values higher than pH_{pzc} (5.3). It generates electrostatic repulsion between the negatively charged adsorbent and MO molecules, consequently decreasing ABPB adsorption capacity. Other interactions may happen among MO molecules and ABPB: pore MO could form hydrogen bonds with oxygen-containing functional groups on ABPB surface, such as C-O, C=O, -OH; π - π interactions between the graphitic structure of the ABPB and the aromatic rings of the MO dye; interaction between H bonds from the OH groups and the delocalized π electron

Table 7

Adsorption isotherm constants for methyl orange (MO) and methylene blue (MB) adsorption by activated birchwood pellet biocarbon (ABPB) (q_m ($mg \cdot g^{-1}$): the maximum adsorption capacity, K_L ($L \cdot mg^{-1}$): Langmuir constant related to the energy of adsorption and affinity of the binding sites, K_F ($mg \cdot g^{-1}$)($L \cdot mg^{-1}$) $^{1/n}$: Freundlich constant representing the adsorption capacity and intensity, $(1/n)$: adsorbent system's favorability and efficiency, a_T ($L \cdot mg^{-1}$): Temkin isotherm constant representing the binding constant reflecting the maximum binding energy, b_T ($J \cdot mol^{-1}$): Temkin constant.

Isotherm model	Dye	MO	MB
Langmuir	q_m (mg/g)	153.99	86.92
	K_L ($L \cdot mg^{-1}$)	0.06	1.19
	R^2	0.7185	0.6932
Freundlich	$1/n$	0.26	0.15
	K_F ($(mg/g)(L/mg)^{1/n}$)	38.46	40.25
	R^2	0.9108	0.9083
Temkin	a_T ($L \cdot mg^{-1}$)	8.01	137.92
	b_T ($J \cdot mol^{-1}$)	132.35	287.42
	R^2	0.7895	0.8322

cloud based on the Yoshida-H bonding mechanism [54]. Overall, it can be concluded that MO adsorption on ABPB may be mainly attributed to numerous mechanisms happening at the same time, and having relative significance depending on conditions below (Fig. 9) and above the pK_a value (Fig. 10) of MO (i.e., 3.46): electrostatic attraction and pore diffusion, hydrogen bonding, Yoshida hydrogen bonding, n - π interaction, π -cation interaction, and π - π stacking.

The adsorption mechanisms for MO and MB are influenced by both chemical interactions and the physical characteristics of the adsorbents. Among these characteristics, the pore size distribution – especially mesoporosity – plays a critical role in the adsorption of larger dye molecules like MO and MB. Although ABPB exhibited lower SSA and micropore volume compared to CAC_{mineral} , its higher external surface area and larger average pore diameter indicate a greater presence of mesopores, which could enhance adsorption. This structural advantage likely explains why ABPB demonstrated higher adsorption capacities for both MO and MB under specific conditions, as larger pores allow for easier diffusion of these molecules into the adsorbent matrix. Studies have shown that adsorbents with higher mesoporosity tend to exhibit improved adsorption for larger molecules like MB. For example, Lawtae and Tangsathikulchai (2021) [55] found that an adsorbent with the highest mesoporosity achieved the greatest adsorption capacity for MB compared to adsorbents with lower mesoporosity. This highlights the importance of having a well-balanced pore structure to optimize adsorption performance, particularly for larger organic molecules. MB adsorption followed Elovich kinetic model, suggesting that chemisorption including external liquid film diffusion, surface adsorption, and intra-particle diffusion processes happen. Moreover, several active functional groups on ABPB are able to form hydrogen bonds with the nitrogen groups in MB [7]. Also, the aromatic structure of the ABPB can bond with the benzene ring in the MB molecules via π - π stacking. Considering the results of the analysis of the zeta potential at different pH values, the highly protonated surface functional groups on ABPB reduced the negatively charged active sites in the acidic solution, which led to a weakened electrostatic attraction between ABPB and the cationic form of MB in solution and inhibited their adsorption. At the same time, decreasing pH increased the H^+ ability to compete with MB for the active sites ABPB surface. On the contrary, the positive charge density on ABPB surface decreased due to deprotonation at greater pH values, thus enhancing the electrostatic attraction to MB. Therefore, due to the significant electrostatic contributions, the adsorption of MB on ABPB can be maximized under alkaline conditions. Overall, the adsorption mechanism of MB onto ABPB is the result of electrostatic interaction, hydrogen bonding, π - π stacking, and physical interaction (surface contact and pore diffusion), as schematically illustrated in Figs. 11 and 12.

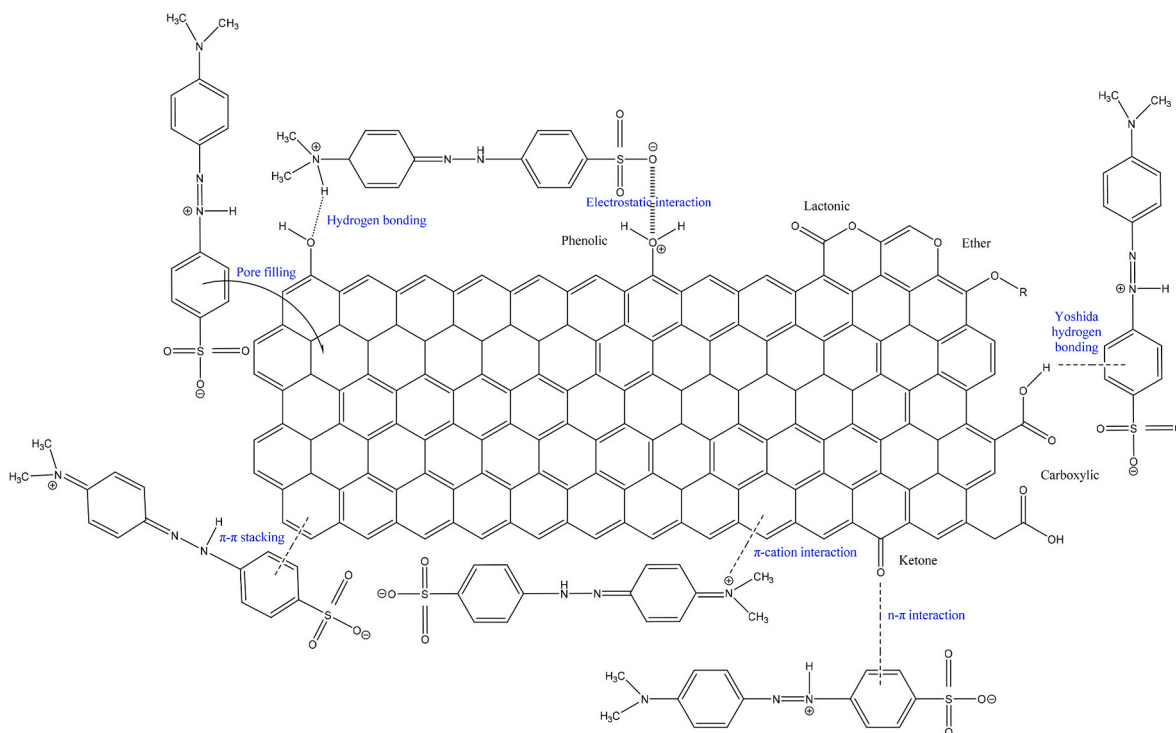


Fig. 9. Possible methyl orange (MO) adsorption mechanisms onto activated birchwood pellet biocarbon (ABPB) below pKa (3.46). (For interpretation of the references to colour in this figure legend, the reader is referred to the Web version of this article.)

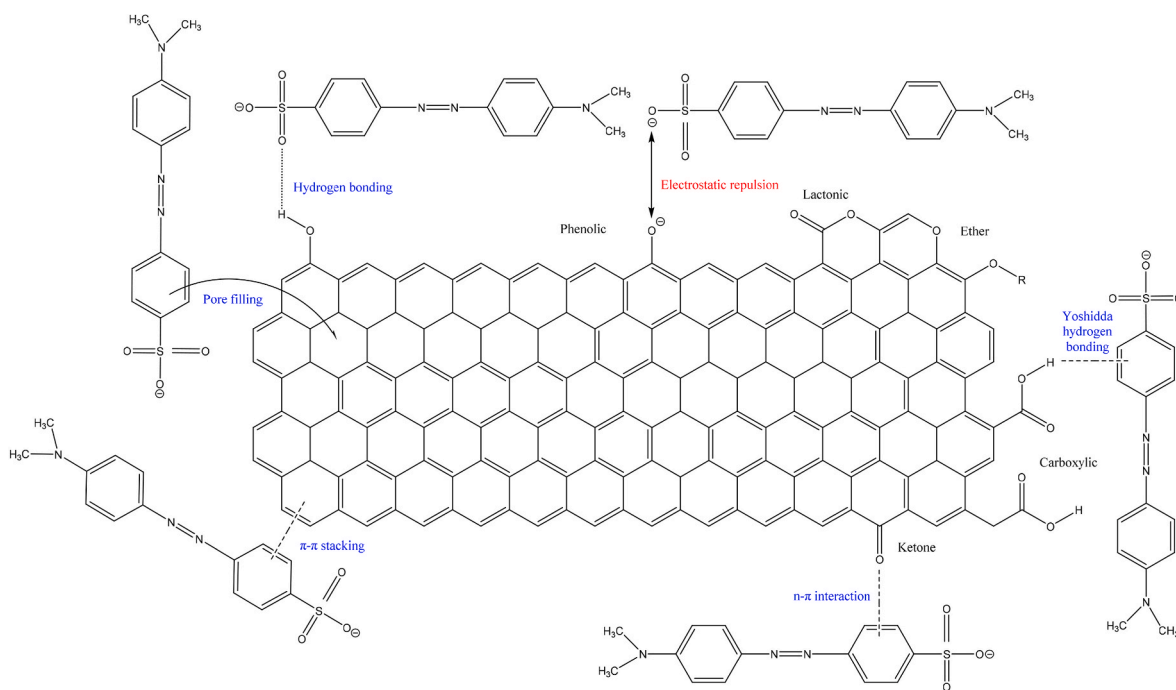


Fig. 10. Possible methyl orange (MO) adsorption mechanisms onto activated birchwood pellet biocarbon (ABPB) above pKa (3.46). (For interpretation of the references to colour in this figure legend, the reader is referred to the Web version of this article.)

4. Conclusions

This study demonstrates the potential of physically activated birchwood pellets biocarbon (ABPB), obtained via pyrolysis and CO_2 activation, as a promising adsorbent for MO and MB under varying pH conditions. Compared to $\text{CAC}_{\text{mineral}}$, ABPB exhibited lower SSA, micropore volume, and total pore volume, but a larger average pore diameter

and higher external surface area, which contributed to its favorable adsorption capacity for both dyes. ABPB achieved a maximum capacity of 220 mg/g for MO and 91 mg/g for MB, with adsorption equilibrium reached within 17 h. Under all tested conditions, ABPB showed either higher or comparable adsorption capacities relative to $\text{CAC}_{\text{mineral}}$. The adsorption mechanisms varied depending on the pH and dye characteristics. For MO, adsorption at pH 2 was driven by electrostatic

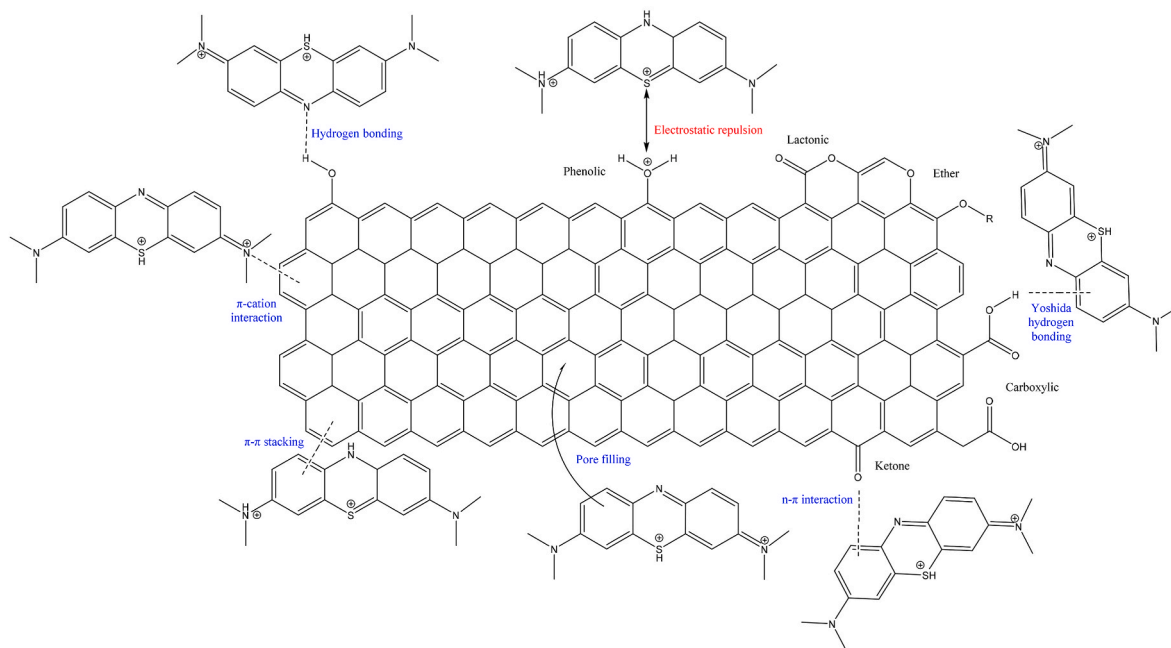


Fig. 11. Possible methylene blue (MB) adsorption mechanisms onto activated birchwood pellet biocarbon (ABPB) below pKa (3.80). (For interpretation of the references to colour in this figure legend, the reader is referred to the Web version of this article.)

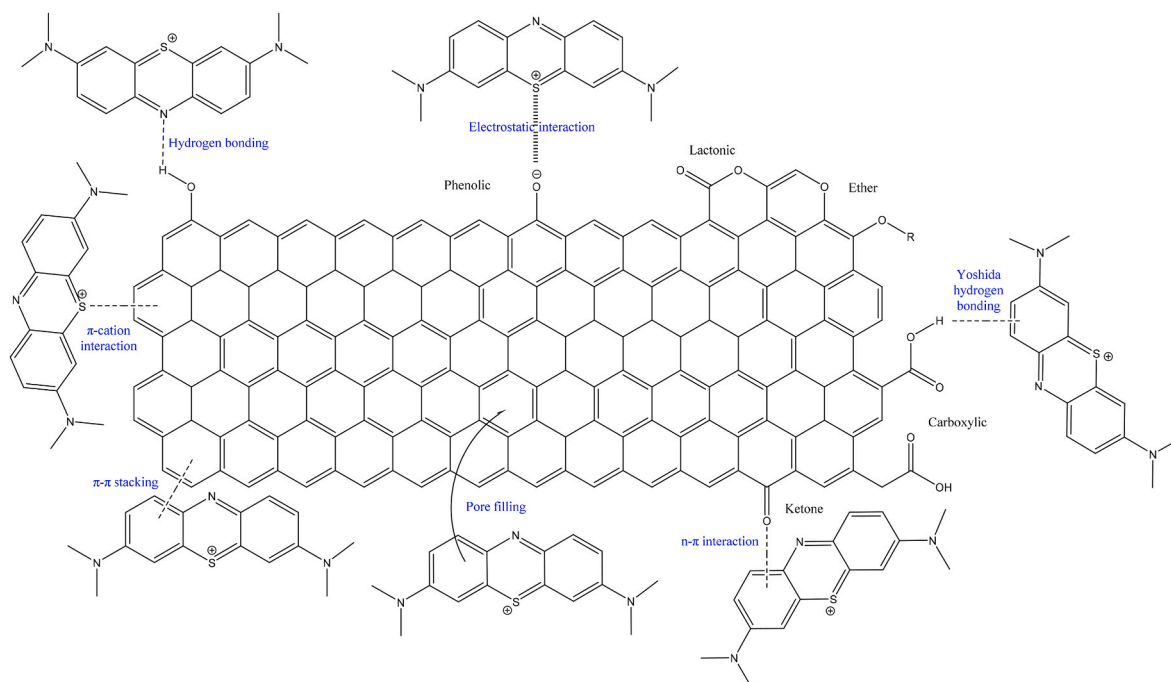


Fig. 12. Possible methylene blue (MB) adsorption mechanisms onto activated birchwood pellet biocarbon (ABPB) above pKa (3.80). (For interpretation of the references to colour in this figure legend, the reader is referred to the Web version of this article.)

attraction and hydrogen bonding, while at higher pH levels, mechanisms such as π - π stacking and pore filling became more significant. For MB, adsorption was primarily influenced by electrostatic interactions and π - π stacking, with ABPB outperforming CAC_{mineral} across all pH levels due to its larger mesopores and stronger surface functional groups. The broader impact of these findings lies in ABPB's potential as a sustainable alternative to CAC_{mineral} , particularly for wastewater treatment applications. Future research should explore the regeneration and reusability of

ABPB, as well as the effects of different feedstocks and activation methods on adsorption performance. Additionally, testing ABPB in real-world wastewater scenarios will help validate its practical applicability and environmental benefits.

CRediT authorship contribution statement

Heejin Lee: Writing – review & editing, Writing – original draft,

Methodology, Investigation, Formal analysis. **Silvia Fiore**: Writing – review & editing, Validation, Supervision, Formal analysis, Conceptualization. **Franco Berruti**: Writing – review & editing, Validation, Supervision, Resources, Project administration, Methodology, Funding acquisition, Formal analysis, Conceptualization.

Acknowledgements

The authors are grateful to the several industry partners and to the Natural Sciences and Engineering Research Council of Canada for financial support of this research through the Industrial Research Chair program.

Data availability

Data will be made available on request.

References

- I.-J. Hwang, T.A. Vo, S.S. Choi, J. Kim, H.T. Hwang, S.-S. Kim, Preparation of activated carbon from ginkgo leaves by steam activation for adsorption application with isotherm and kinetics, *Biomass Bioenergy* 182 (2024) 107097, <https://doi.org/10.1016/j.biombioe.2024.107097>.
- Y. Liu, Y. Cao, Q. Yu, In-situ deep eutectic solvent enhance hydrothermal carbonization of garden waste for methylene blue removal, *Biomass Bioenergy* 167 (2022) 106626, <https://doi.org/10.1016/j.biombioe.2022.106626>.
- T.R. Brazil, M. Gonçalves, M.S.O. Junior, M.C. Rezende, Sustainable process to produce activated carbon from Kraft lignin impregnated with H₃PO₄ using microwave pyrolysis, *Biomass Bioenergy* 156 (2022) 106333, <https://doi.org/10.1016/j.biombioe.2021.106333>.
- K. Philippou, I. Anastopoulos, C. Dosche, I. Pashalidis, Synthesis and characterization of a novel Fe₃O₄-loaded oxidized biochar from pine needles and its application for uranium removal. Kinetic, thermodynamic, and mechanistic analysis, *J. Environ. Manage.* 252 (2019) 109677, <https://doi.org/10.1016/j.jenvman.2019.109677>.
- Global activated carbon market size/share worth USD 9.4 billion by 2032 at a 5.3% CAGR: custom market insights. <https://www.lib.uwo.ca/cgi-bin/ezpauthn.cgi>, 2024. <http://search.proquest.com/wire-feeds/latest-global-activated-carbon-market-size-share/docview/2931750128/se-2?accountid=15115>.
- S. Sahu, S. Pahi, S. Tripathy, S.K. Singh, A. Behera, U.K. Sahu, R.K. Patel, Adsorption of methylene blue on chemically modified lychee seed biochar: dynamic, equilibrium, and thermodynamic study, *J. Mol. Liq.* 315 (2020) 113743, <https://doi.org/10.1016/j.molliq.2020.113743>.
- N. Suhaimi, M.R.R. Kooh, C.M. Lim, C.-T. Chou Chao, Y.-F. Chou Chau, A. H. Mahadi, H.-P. Chiang, N.H. Haji Hassan, R. Thotagamuge, The use of gigantochloa bamboo-derived biochar for the removal of methylene blue from aqueous solution, *Adsorpt. Sci. Technol.* 2022 (2022) 1–12, <https://doi.org/10.1155/2022/8245797>.
- R.B.N. Lekene, T.M.M. Ntep, M.N.A. Fetzer, T. Strothmann, J.N. Nsami, C. Janiak, The efficient removal of ibuprofen, caffeine, and bisphenol A using engineered egusi seed shells biochar: adsorption kinetics, equilibrium, thermodynamics, and mechanism, *Environ. Sci. Pollut. Res.* 30 (2023) 100095–100113, <https://doi.org/10.1007/s11356-023-29377-w>.
- K. Sun, J.C. Jiang, Preparation and characterization of activated carbon from rubber-seed shell by physical activation with steam, *Biomass Bioenergy* 34 (2010) 539–544, <https://doi.org/10.1016/j.biombioe.2009.12.020>.
- L. Liu, S. Shi, H. Hu, Y. Huang, Investigation of phenol adsorption performance and mechanism using Na₂EDTA-modified activated biochars produced from a fluidized bed pyrolysis system, *Biomass Bioenergy* 183 (2024) 107164, <https://doi.org/10.1016/j.biombioe.2024.107164>.
- J. Mokrzycki, A. Magdziarz, P. Rutkowski, The influence of the Miscanthus giganteus pyrolysis temperature on the application of obtained biochars as solid biofuels and precursors of high surface area activated carbons, *Biomass Bioenergy* 164 (2022) 106550, <https://doi.org/10.1016/j.biombioe.2022.106550>.
- Y.W. Low, K.F. Yee, A review on lignocellulosic biomass waste into biochar-derived catalyst: current conversion techniques, sustainable applications and challenges, *Biomass Bioenergy* 154 (2021) 106245, <https://doi.org/10.1016/j.biombioe.2021.106245>.
- C. Diaz-Urbe, J. Ortiz, F. Duran, W. Vallejo, J. Fals, Methyl orange adsorption on biochar obtained from prosopis juliflora waste: thermodynamic and kinetic study, *ChemEngineering* 7 (2023) 114, <https://doi.org/10.3390/chemengineering7060114>.
- H. Zeghioud, L. Fryda, A. Mahieu, R. Visser, A. Kane, Potential of flax shives and beech wood-derived biochar in methylene blue and carbamazepine removal from aqueous solutions, *Materials* 15 (2022) 2824, <https://doi.org/10.3390/ma15082824>.
- D. Dang, L. Mei, G. Yan, W. Liu, Synthesis of nanoporous biochar from rice husk for adsorption of methylene blue, *J. Chem.* 2023 (2023) 1–11, <https://doi.org/10.1155/2023/6624295>.
- G.V. Serban, V.I. Iancu, C. Dinu, A. Tenea, N. Vasilache, I. Cristea, M. Niculescu, I. Ionescu, F.L. Chiriac, Removal efficiency and adsorption kinetics of methyl orange from wastewater by commercial activated carbon, *Sustainability* 15 (2023) 12939, <https://doi.org/10.3390/su151712939>.
- M.T. Amin, A.A. Alazba, M. Shafiq, Successful application of Eucalyptus camdulensis biochar in the batch adsorption of crystal violet and methylene blue dyes from aqueous solution, *Sustainability* 13 (2021) 3600, <https://doi.org/10.3390/su13073600>.
- Y. Lu, Y. Liu, C. Li, H. Liu, H. Liu, Y. Tang, C. Tang, A. Wang, C. Wang, Adsorption characteristics and mechanism of methylene blue in water by NaOH-modified areca residue biochar, *Processes* 10 (2022) 2729, <https://doi.org/10.3390/pr10122729>.
- S. Liu, C. Shen, Y. Wang, Y. Huang, X. Hu, B. Li, Karnowo, J. Zhou, S. Zhang, H. Zhang, Development of CO₂/H₂O activated biochar derived from pine pyrolysis: application in methylene blue adsorption, *J. Chem. Technol. Biotechnol.* 97 (2022) 885–893, <https://doi.org/10.1002/jctb.6971>.
- X. Cai, T. Shi, C. Yu, R. Liao, J. Ren, Sorption characteristics of methylene blue on medulla tetrapanacis biochar and its activation technology, *Water. Air. Soil Pollut.* 234 (2023) 223, <https://doi.org/10.1007/s11270-023-06250-7>.
- Y. Xu, Y. Liu, S. Liu, X. Tan, G. Zeng, W. Zeng, Y. Ding, W. Cao, B. Zheng, Enhanced adsorption of methylene blue by citric acid modification of biochar derived from water hyacinth (*Eichornia crassipes*), *Environ. Sci. Pollut. Res.* 23 (2016) 23606–23618, <https://doi.org/10.1007/s11356-016-7572-6>.
- M.A. Hassaan, M. Yilmaz, M. Helal, M.A. El-Nemr, S. Ragab, A. El Nemr, Isotherm and kinetic investigations of sawdust-based biochar modified by ammonia to remove methylene blue from water, *Sci. Rep.* 13 (2023) 12724, <https://doi.org/10.1038/s41598-023-39971-0>.
- L. Sunthar, T. Asharp, K. Nadarajah, Insights into mechanisms of novel engineered biochar derived from neem chips via iron catalyst for the removal of methyl orange from aqueous phase, *Water. Air. Soil Pollut.* 234 (2023) 178, <https://doi.org/10.1007/s11270-023-06187-x>.
- B. Zhang, Y. Wu, L. Cha, Removal of methyl orange dye using activated biochar derived from pomelo peel wastes: performance, isotherm, and kinetic studies, *J. Dispers. Sci. Technol.* 41 (2020) 125–136, <https://doi.org/10.1080/01932691.2018.1561298>.
- M. Zubair, N.D. Mu'azu, N. Jarrah, N.I. Blaisi, H.A. Aziz, M.A. Al-Harhi, Adsorption behavior and mechanism of methylene blue, crystal violet, eriochrome black T, and methyl orange dyes onto biochar-derived date palm fronds waste produced at different pyrolysis conditions, *Water. Air. Soil Pollut.* 231 (2020) 240, <https://doi.org/10.1007/s11270-020-04595-x>.
- MdS. Islam, H. Roy, S. Afrose, Phosphoric acid surface modified *Moringa oleifera* leaves biochar for the sequestration of methyl orange from aqueous solution: characterizations, isotherm, and kinetics analysis, *Remediat. J.* 32 (2022) 281–298, <https://doi.org/10.1002/rem.21733>.
- C. Tcheka, M.M. Conradie, V.A. Assinale, J. Conradie, Mesoporous biochar derived from Egyptian doum palm (*Hyphaene thebaica*) shells as low-cost and biodegradable adsorbent for the removal of methyl orange dye: characterization, kinetic and adsorption mechanism, *Chem. Phys. Impact* 8 (2024) 100446, <https://doi.org/10.1016/j.chphi.2023.100446>.
- J. Chen, C. Tang, X. Li, J. Sun, Y. Liu, W. Huang, A. Wang, Y. Lu, Preparation and modification of rape straw biochar and its adsorption characteristics for methylene blue in water, *Water* 14 (2022) 3761, <https://doi.org/10.3390/w14223761>.
- Y.M. Riyad, T.M. Elmorsi, M.G. Alam, B. Abel, Surface functionalization of bioactive hybrid adsorbents for enhanced adsorption of organic dyes, *Int. J. Environ. Res. Public Health* 20 (2023) 5750, <https://doi.org/10.3390/ijerph20095750>.
- S. Dawood, T.K. Sen, C. Phan, Performance and dynamic modelling of biochar and kaolin packed bed adsorption column for aqueous phase methylene blue (MB) dye removal, *Environ. Technol.* 40 (2019) 3762–3772, <https://doi.org/10.1080/09593330.2018.1491065>.
- J.M. Jabar, Y.A. Odusote, Y.T. Ayinde, M. Yilmaz, African almond (*Terminalia catappa* L) leaves biochar prepared through pyrolysis using H₃PO₄ as chemical activator for sequestration of methylene blue dye, *Results Eng* 14 (2022) 100385, <https://doi.org/10.1016/j.rineng.2022.100385>.
- S.-K. Ahn, K.-Y. Park, W. Song, Y. Park, J.-H. Kweon, Adsorption mechanisms on perfluorooctanoic acid by FeCl₃ modified granular activated carbon in aqueous solutions, *Chemosphere* 303 (2022) 134965, <https://doi.org/10.1016/j.chemosphere.2022.134965>.
- D. De, S. Santosha, V. Aniya, A. Sreeramou, S. B, Assessing the applicability of an agro-industrial waste to Engineered Bio-char as a dynamic adsorbent for Fluoride Sorption, *J. Environ. Chem. Eng.* 6 (2018) 2998–3009, <https://doi.org/10.1016/j.jece.2018.04.021>.
- T. Atugoda, C. Gunawardane, M. Ahmad, M. Vithanage, Mechanistic interaction of ciprofloxacin on zeolite modified seaweed (*Sargassum crassifolium*) derived biochar: kinetics, isotherm and thermodynamics, *Chemosphere* 281 (2021) 130676, <https://doi.org/10.1016/j.chemosphere.2021.130676>.
- D.S. Martins, B.R. Estevam, I.D. Perez, J.H.P. Américo-Pinheiro, W.D. Isique, R. F. Boina, Sludge from a water treatment plant as an adsorbent of endocrine disruptors, *J. Environ. Chem. Eng.* 10 (2022) 108090, <https://doi.org/10.1016/j.jece.2022.108090>.
- Y. Cai, W. Jiang, D. Liu, C. Chang, Adsorption of sulfanilamides using biochar derived from Suaeda salsa: adsorption kinetics, isotherm, thermodynamics, and mechanism, *Environ. Sci. Pollut. Res.* 30 (2023) 70528–70540, <https://doi.org/10.1007/s11356-023-27228-2>.
- Z. Yang, J. Hou, L. Miao, J. Wu, Comparison of adsorption behavior studies of methylene blue by microalga residue and its biochars produced at different

- pyrolytic temperatures, *Environ. Sci. Pollut. Res.* 28 (2021) 14028–14040, <https://doi.org/10.1007/s11356-020-11470-z>.
- [38] S. Mouhamadou, S. Dalhatou, N. Dobe, R. Djakba, O.O. Fasanya, N.D. Bansod, G. Fita, C.H. Ngayam, J.P.N. Tejeogue, M. Harouna, Linear and non-linear modelling of kinetics and equilibrium data for Cr(VI) adsorption by activated carbon prepared from *piliostigma reticulatum*, *Chem. Afr.* 6 (2023) 719–731, <https://doi.org/10.1007/s42250-022-00324-5>.
- [39] J. Lykiema, K.S.W. Sing, J. Haber, M. Kerker, E. Wolfram, J.H. Block, N. V. Churaev, D.H. Everett, R.S. Hansen, R.A.W. Haul, J.W. Hightower, R.J. Hunter, Prepared for Publication by the Subcommittee on Reporting Gas Adsorption Data Consisting of K. S. W. SING (UK, Chairman); D. H. EVERETT (UK); R. A. W. HAUL (FRG); L. MOSCOU (Netherlands); R. A. PIEROTTI (USA); J. ROUQUEROL (France); T. SIEMIENIEWSKA (Poland), 1984.
- [40] N.X. Loc, P.T.T. Tuyen, L.C. Mai, D.T.M. Phuong, Chitosan-Modified biochar and unmodified biochar for methyl orange: adsorption characteristics and mechanism exploration, *Toxics* 10 (2022) 500, <https://doi.org/10.3390/toxics10090500>.
- [41] S. Chen, M. Zhou, H.-F. Wang, T. Wang, X.-S. Wang, H.-B. Hou, B.-Y. Song, Adsorption of reactive brilliant red X-3B in aqueous solutions on clay–biochar composites from bagasse and natural attapulgite, *Water* 10 (2018) 703, <https://doi.org/10.3390/w10060703>.
- [42] A.K. Yadav, A.K. Chaubey, S. Kapoor, T. Pratap, B. Preetiva, V. Vimal, D. Mohan, Sustainable napier grass (*pennisetum purpureum*) biochar for the sorptive removal of acid orange 7 (AO7) from water, *Processes* 12 (2024) 1115, <https://doi.org/10.3390/pr12061115>.
- [43] M. Singh, Mohd Ahsan, V. Pandey, A. Singh, D. Mishra, N. Tiwari, P. Singh, T. Karak, P. Khare, Comparative assessment for removal of anionic dye from water by different waste-derived biochar vis a vis reusability of generated sludge, *Biochar* 4 (2022) 13, <https://doi.org/10.1007/s42773-022-00140-7>.
- [44] W. Huang, J. Chen, J. Zhang, Adsorption characteristics of methylene blue by biochar prepared using sheep, rabbit and pig manure, *Environ. Sci. Pollut. Res.* 25 (2018) 29256–29266, <https://doi.org/10.1007/s11356-018-2906-1>.
- [45] K. Wystalska, A. Kwarciak-Kozłowska, Utilization of digestate from agricultural and food waste for the production of biochar used to remove methylene blue, *Sustainability* 15 (2023) 14723, <https://doi.org/10.3390/su152014723>.
- [46] D.D. Sewu, P. Boakye, H. Jung, S.H. Woo, Synergistic dye adsorption by biochar from co-pyrolysis of spent mushroom substrate and *Saccharina japonica*, *Bioresour. Technol.* 244 (2017) 1142–1149, <https://doi.org/10.1016/j.biortech.2017.08.103>.
- [47] P. Singh, R. Kumar, R. Kumari, N.B. Singh, R.C. Singh, P.K. Singh, Methylene blue dye removal from water by neem leaf (*Azadirachta indica*) adsorbent, *Macromol. Symp.* 407 (2023) 2200069, <https://doi.org/10.1002/masy.202200069>.
- [48] N. Chaukura, E.C. Murimba, W. Gwenzi, Synthesis, characterisation and methyl orange adsorption capacity of ferric oxide–biochar nano-composites derived from pulp and paper sludge, *Appl. Water Sci.* 7 (2017) 2175–2186, <https://doi.org/10.1007/s13201-016-0392-5>.
- [49] L. Liu, Y. Li, S. Fan, Preparation of KOH and H3PO4 modified biochar and its application in methylene blue removal from aqueous solution, *Processes* 7 (2019) 891, <https://doi.org/10.3390/pr7120891>.
- [50] H. Nath, A. Saikia, P.J. Goutam, B.K. Saikia, N. Saikia, Removal of methylene blue from water using okra (*Abelmoschus esculentus* L.) mucilage modified biochar, *Bioresour. Technol. Rep.* 14 (2021) 100689, <https://doi.org/10.1016/j.biteb.2021.100689>.
- [51] J. Wang, W. Chen, M. Zhang, R. Zhou, J. Li, W. Zhao, L. Wang, Optimize the preparation of Fe3O4-modified magnetic mesoporous biochar and its removal of methyl orange in wastewater, *Environ. Monit. Assess.* 193 (2021) 179, <https://doi.org/10.1007/s10661-021-08971-w>.
- [52] S. Fan, J. Tang, Y. Wang, H. Li, H. Zhang, J. Tang, Z. Wang, X. Li, Biochar prepared from co-pyrolysis of municipal sewage sludge and tea waste for the adsorption of methylene blue from aqueous solutions: kinetics, isotherm, thermodynamic and mechanism, *J. Mol. Liq.* 220 (2016) 432–441, <https://doi.org/10.1016/j.molliq.2016.04.107>.
- [53] Z. Wu, X. Wang, J. Yao, S. Zhan, H. Li, J. Zhang, Z. Qiu, Synthesis of polyethyleneimine modified CoFe2O4-loaded porous biochar for selective adsorption properties towards dyes and exploration of interaction mechanisms, *Sep. Purif. Technol.* 277 (2021) 119474, <https://doi.org/10.1016/j.seppur.2021.119474>.
- [54] N.H.M. Yusoff, C.H. Chong, V.L. Wong, K.H. Cheah, Y.K. Wan, The influence of structural topology of additively manufactured PEGDA monolith on adsorption performance for textile wastewater treatment, *Asia Pac. J. Chem. Eng.* 18 (2023) e2952, <https://doi.org/10.1002/apj.2952>.
- [55] P. Lawtae, C. Tangsathitkulchai, The use of high surface area mesoporous-activated carbon from longan seed biomass for increasing capacity and kinetics of methylene blue adsorption from aqueous solution, *Molecules* 26 (2021) 6521, <https://doi.org/10.3390/molecules26216521>.